Chemical Engineering Journal 442 (2022) 135925

Contents lists available at ScienceDirect

Chemical Engineering Journal

journal homepage: www.elsevier.com/locate/cej

Extrusion-free fabrication of zinc-rich powder coatings: Press bonding

Jinbao Huang [a], Marshall Yang [a], Wenhao Zhu [a], Keyong Tang [b], Hui Zhang [a,*], Jian Chen [c], James J. Noël [c], Ivan Barker [d], Haiping Zhang [e], Jesse Zhu [a]

[a] Department of Chemical and Biochemical Engineering, Western University, London, ON N6A 5B9, Canada
[b] School of Materials Science and Engineering, Zhengzhou University, Zhengzhou 450001, China
[c] Department of Chemistry, The University of Western Ontario, London N6A 5B7, Canada
[d] Surface Science Western, The University of Western Ontario, London N6G 0J3, Canada
[e] School of Chemical Engineering and Technology, Tianjin University, Tianjin 300350, China

ARTICLE INFO

Keywords:
Extrusion-free
Zinc-rich
Powder coatings
Corrosion protection
Press bonding

ABSTRACT

Given their environmental benefits, zinc-rich powder coatings (ZRPCs) have been used to replace their solvent-based counterparts. However, current ZRPCs can load only 70 wt% zinc, and therefore cannot meet higher anti-corrosive requirements where the zinc concentration is usually over 80 wt%. Above 70 wt% zinc, powder coatings manufacturers encounter problems with powder homogeneity and extruder screw wear. Here, we demonstrate for the first time an extrusion-free method to fabricate ZRPCs by employing a press to avoid using the extruder. The binder and zinc particles formed a raspberry-like zinc-on-binder structure after press bonding. The zinc dust content can reach about 90 wt% in the coating powders. In addition, the press-bonded zinc-rich coating films with 80 wt% zinc showed slightly lower barrier effects, but a more uniform dispersion of zinc particles and a higher zinc utilization and in turn, longer cathodic protection (110 days), narrower corrosion creepage and fewer localized corrosion sites than the extruded coating films (101 days) with the same zinc content.

1. Introduction

Zinc-rich coatings have been extensively used for decades to protect steel from corrosion [1]. They can be used for many applications including commercial buildings, bridges [2], industrial ports [3], oil and gas pipeline [4], and wind turbines [5]. In zinc-rich coatings, more electrochemically active zinc particles behave as anodes and sacrifice themselves to provide cathodic protection to the steel substrate [6]. The corrosion performance of these zinc-rich coatings mainly relies on the flow of galvanic current between zinc particles and the steel substrate [2]. As long as there is sufficient electrical connection between zinc particles and the substrate, the steel will be galvanically protected. Hence, the zinc contents of these zinc-rich coatings are usually required to be very high, which is at least 65 wt% and could be up to 93 wt% of the dry film for liquid coatings [7]. When the galvanic circuit is broken and the cathodic protection fails, the zinc-rich coatings can still protect the substrate due to the formation of zinc corrosion products acting as reinforced corrosion barriers [6,8].

Most of the zinc-rich coatings are based on liquid coatings. A big concern of zinc-rich liquid coatings is the usage of volatile organic compounds (VOCs), which contribute to environmental pollution. Since the 1970s, powder coatings have been preferred because their all-solid composition provides environmental benefits [9]. More recently, zinc-rich powder coatings have been reported [10] and used in industry, but the concentrations of zinc particles (or dust) in these zinc-rich powder coatings were far below 80 wt%, which is usually required for the solvent-based counterparts to provide sufficient corrosion protection to the steel substrates in aggressive environments [10,11].

To manufacture zinc-rich powder coatings, zinc dust and polymer binders are subjected to extrusion when screws vigorously mix the melted binders and zinc dust. Zinc-rich powder coatings with zinc concentrations above 70 wt% will cause problems for manufacturers in terms of powder homogeneity [11]. When the coating is cured, zinc-rich and zinc depleted areas are formed inside the coating film. Indeed, 80 wt % of zinc particles account for 36 vol% of the total volume, while 90 wt % of zinc particles occupy 56 vol%. With such high pigment loads, the extrusion can be difficult or even impossible. These coating manufacture processes may severely wear or even damage the screws, which are the

* Corresponding author.
E-mail address: hzhang1@uwo.ca (H. Zhang).

https://doi.org/10.1016/j.cej.2022.135925
Received 1 October 2021; Received in revised form 5 March 2022; Accepted 19 March 2022
Available online 29 March 2022
1385-8947/

most essential and expensive component of an extruder.

The traditional method for solving the problems of screw wear and zinc inhomogeneity is to decrease the zinc particle concentration by, for example, replacing some of the spherical zinc particles with lamellar zinc flakes [1,12]. Zinc flakes have a higher specific surface area than the spherical zinc particles and provide a greater barrier effect [1], but the reactivity of zinc flakes is too high to offer long-term protection [12]. To make full use of the zinc particles inside the coating and improve the electrical connection of zinc to the steel substrate, researchers have proposed incorporating conductive additives such as carbon black [10,13] conductive polymers [14,15], clay [16,17], nano-zinc [18,19], graphene [20-22], and carbon nanotubes [23]. The upper limit of anti-corrosive properties is based on the full use of the existing zinc dust in the coating.

However, these approaches are all based on a reduced zinc content. They represent the first one of the two options: the better usage of zinc and/or a higher inventory of zinc in coating film. In this work, the second option augmenting the limit to the zinc content was explored. Since press bonding has been widely used to bond solid fine particles in powder metallurgy and in the preparation of pharmaceuticals [24-27], it could be utilized to fabricate the zinc-rich power coating with a high zinc content (i.e., $\geq$ 80 wt%). To the best of our knowledge, zinc-rich powder coatings with zinc concentration of $\geq$ 80 wt%, which are expected to have better corrosion performance, have never been reported. In the present work, a tablet press was employed to bond zinc particles and polymer binder instead of an extruder. The binder is a commercial polyester clearcoat powder coating possessing a good outdoor durability. After these zinc-rich power coatings were fabricated, their bonding performance, surface morphologies, dispersion of zinc particles and corrosion performances were characterized, evaluated, and compared to the extruded zinc-rich coating film.

2. Experimental

2.1. Materials

Polyester clear coat powder coatings procured from TCI Powder Coatings Co., Ltd., (USA) were used as the base binder system. Zinc dust (approximately 5 μm in average particle size) purchased from North Zinc Dust (Canada) was used as the sacrificial anode. Standard Q-panel steel panels purchased from Q-Lab Corporation (USA) were the substrates. Sulfuric acid from Fisher Scientific (USA) was utilized as the reagent with zinc for gas-volumetric analysis.

2.2. Preparation of press-bonded powders and coated panels

The fabrication process of press-bonded powder coatings is illustrated in Fig. 1. Polyester clearcoat powder with a median particle size (D50) of 46 μm was firstly pulverized into ultrafine (D50 = 13 μm) and fine particles (D50 = 30 μm), respectively. The particle size distribution was measured with a laser particle size analyzer (BT-2000B) from Bettersize Instruments Lt. (China). The obtained binder powders were thoroughly mixed with zinc dust before press bonding. Typically, 80 g of zinc dust was combined with 20 g binder to prepare the 80 wt% press-bonded zinc-rich coatings.

During the press bonding process (Fig. 1), the zinc-rich mixture was loaded into a stainless-steel cylinder, which was pressed under 9 tons force on a 3.14 cm^2 cylinder inner area. The powder mixture became a grey tablet with metallic luster as shown in Fig. S1. For comparison, polyester clearcoat powder was mixed with zinc dust and extruded with a twin-screw extruder (SLJ-10) from Yantai Donghui Powder Processing Equipment Co., Ltd. (China). The screw speed was 300 rpm, and the temperature was 120 °C.

The pressed tablets and extruded chips were ground and sifted to obtain coating powders, which were then sprayed and cured onto a steel substrate. Spraying was done with an electrostatic spraying gun (ITW Gema, Switzerland) in a powder coating spraying booth (N902, Nordson Corporation, USA) at 70 kV and 15 cm away from the grounded substrate. During spraying, the particles were charged by an electrostatic gun and flew towards the substrate with the compressed air [9]. Finally, all coated panels were cured at 200 °C for 15 min. During curing, the particles melted and leveled. The resin and curing agent quickly cross-linked. The dry film thickness of the obtained coating film was about 40.0 μm, as measured with a thickness gauge (Positector 6000) from

Table 1
The symbols of the prepared zinc-rich powders and coatings.

	Process	Zinc (wt. %)	Binder (wt. %)	D50 of binder particles (μm)
E80	Extrusion	80	20	N/A
P80uf	Press bonding	80	20	13.0
P80f	Press bonding	80	20	28.6
P80C	Press bonding	80	20	48.9
P85uf	Press bonding	85	15	13.0
P90uf	Press bonding	90	10	13.0

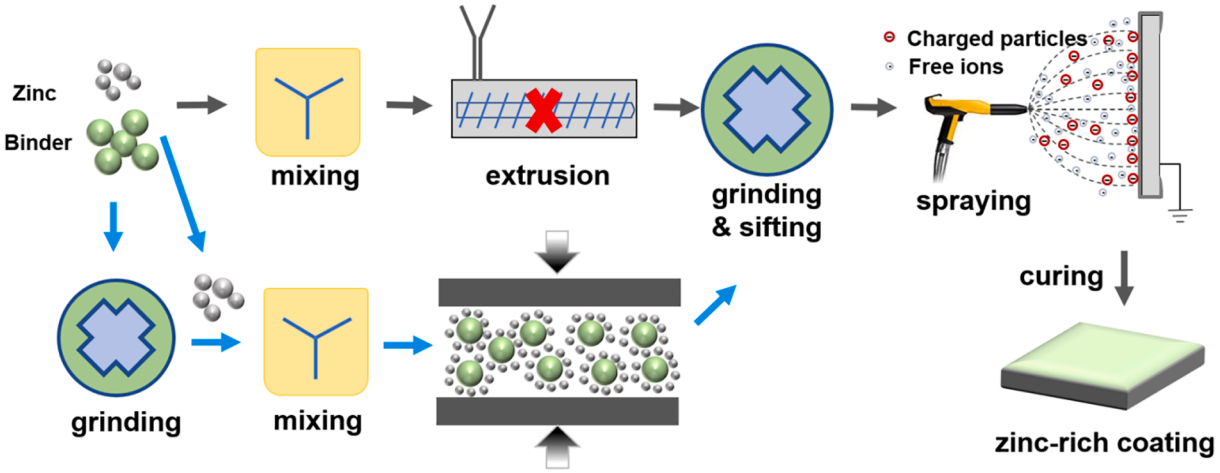

Fig. 1. Sketch for the proposed fabrication of ZRPC with press bonding.

Defeisko Co. (USA). The symbols of the prepared zinc-rich powders and coatings are listed in Table 1.

2.3. Characterization of the press-bonded powders

During electrostatic spraying, non-bonded zinc particles will separate with the coating powder because of charge abilities, and cause zinc content differences between the original powder and the deposited powder. A closer zinc content between P90uf and Deposited P90uf represents better bonding. To evaluate the bonding performance of press-bonded coating powders, the P90uf powders were selected as the representative material because this one has the highest zinc concentration and is the most challenging for press bonding. The powders were first sprayed onto and then carefully scraped off the grounded substrate. The scraped powder was named "Deposited P90uf". The zinc contents in P90uf and Deposited P90uf powders were evaluated with the gas-volumetric method [28]. Dilute sulfuric acid was utilized to react with zinc and produce hydrogen, which propelled water out of a water-filled bottle. Then the zinc content in the sample could be measured using the volume of water. The involved chemical reaction is shown as:

$$Zn\ (s) + H_2SO_4(l) = ZnSO_4 + H_2\ (g) \quad (1)$$

By using Eq. (1), the zinc content of the powdered sample could be calculated as:

$$\omega = \frac{V_{H_2} M_{Zn}}{V_m m_{sample}} \times 100\% \quad (2)$$

where ω is the content of zinc; V_{H_2} is the volume of hydrogen, which was determined from the volume of the expelled water; M_{Zn} is the relative atomic mass of zinc; V_m is the molar volume of hydrogen at 25 °C and 1 atm; m_{sample} is the total mass of a powder sample.

The zinc dust used for anti-corrosive paints usually has 3–5 % impurities. To get the bonded zinc dust content in the coating, the original zinc dust was used as the reference powder. The zinc content of the reference powder was labeled as ω_{dust}. The bonded zinc dust in the coating was deduced as:

$$\varphi = \frac{\omega_{sample}}{\omega_{dust}} \times 100\% \quad (3)$$

where φ is the zinc dust content in the coating; ω_{sample} is the zinc content of a powdered sample. The chemical analysis set up employed to measure the zinc content was shown in Fig. S2. Pressure tightness was verified before each test. Three measurements gave the mean. In this way, the zinc dust content in P90uf and deposited P90uf powders was obtained.

The morphology of coating powders was characterized with a scanning electron microscope (SEM, S3900, Hitachi, Japan) under an accelerating voltage of 10 kV. Gold sputtering was performed before observation for better resolution.

To calculate the volumetric percentage of the zinc inside a coating or powder, the following equation was used:

$$\delta_{zinc} = \frac{\frac{W_{zinc}}{\rho_{zinc}}}{\frac{W_{zinc}}{\rho_{zinc}} + \frac{W_{binder}}{\rho_{binder}}} \times 100\% \quad (4)$$

where δ_{zinc} is the volume of zinc in the mixture; W_{zinc} the weight ratio of zinc; ρ_{zinc} the density of zinc (7.1 g/cm^3); W_{binder} the weight ratio of binder; and ρ_{binder} the density of clearcoat binder (1.0 g/cm^3).

2.4. Surface and cross-sectional morphologies

To evaluate the surface quality of the fabricated coatings, Rhopoint IQ 20/60 gloss meter (Rhopoint Instruments Ltd., UK) was employed to measure the specular gloss (ASTM D523 – 14). The surface morphology was characterized with CLSM (LSM 900, Carl Zeiss Microscopy GmbH, Jena, Germany) to obtain a detailed surface map. The acquired data were processed by the software ConfoMap version 7.4.8341, which provided surface images and roughness.

To characterize the dispersion of zinc particles inside the coating films, optical microscopy (OM, Keyence VHX-950F, Zeiss, Germany) was employed to observe from the top of the coating films. In addition, the coated panels were cut into pieces and mounted in epoxy to observe the cross-sectional morphologies. Then the whole mounting was ground and polished before being characterized by SEM. Micro-CT (X-ray micro computed tomography, Zeiss Xradia 410 Versa Micro-CT, Germany) was used to obtain a 3D view of the zinc particle dispersion.

2.5. Corrosion tests

The corrosion performances of the extruded and press-bonded ZRPCs were investigated with neutral salt spray tests, potentiodynamic polarization tests and electrochemical impedance spectroscopy (EIS) measurements. The salt spray tests (ASTM B117-16) were performed in a salt spray chamber (MX-9204, Associated Environmental Systems, USA). Two 0.5 mm intersecting scribes were made on the coating panels prior to the tests. The performance was evaluated as per ISO 4628–8 after each 500 h of exposure. The panels for electrochemical tests were immersed in a tank filled with 3.5 wt% NaCl solution. A panel was pulled out before it was sent to and returned to the tank after each electrochemical test [29]. Potentiodynamic polarization tests and EIS measurements were carried out on a Modulab (Solartron) electrochemical workstation in 3.5 wt% NaCl solution in a three-electrode system. A saturated calomel electrode (SCE) worked as reference electrode, a platinum foil as counter electrode, and the coated panel as working electrode. The exposed area of the coating panels was 20.25 cm^2. EIS measurements were conducted from 10^5 Hz to 0.01 Hz with a sinusoidal voltage amplitude of 20 mV. EIS results were fitted with Zview software to record corrosion parameters. The potentiodynamic polarization test was measured from −250 mV to + 250 mV vs. open circuit potential (OCP) at a scanning rate of 1 mV/s.

3. Results and discussion

3.1. Press bonding performance

Zinc and binder particles have different electrostatic charge capacities, which can lead to different transfer rates between zinc and binder particles [30]. Varied metal contents can cause inconsistence in coating qualities, which is very common in metallic pigmented powder coatings [31-33]. In zinc-rich coatings, zinc content is a key factor for the final anti-corrosive performances. The first and most important step is to evaluate the bonding performance of the press-bonded powders, which can be evaluated by the difference in zinc contents between the original and the deposited powders. Similar zinc contents indicate that zinc and binder are well bonded.

In pressing, polymer particles deform and bond zinc particles. As zinc particles (5 μm) are much smaller than binder particles (more than 13 μm), zinc tends to be embedded into the binder particles. The smaller binder particles can bond more zinc particles due to their higher specific surface areas compared to the bigger binder particles. It is assumed that the surface of each binder particle is fully covered with half embedded zinc particles. Then the surface area of a binder particle is approximately equal to the total areas of the great circles of all the attached zinc particles. Fig. 2a illustrates the pattern of a bonded particle. To calculate the theoretical zinc loading capacity of a group of binder particles, it is assumed that the surface of each binder particle is fully covered with half embedded zinc particles. The surface area of a binder particle is equal to the total areas of the great circles of all the attached zinc particles. Fig. 2a illustrates the pattern of a bonded particle. The number of loaded zinc particles on each binder particle (N_{zinc}) can be calculated with the equation:

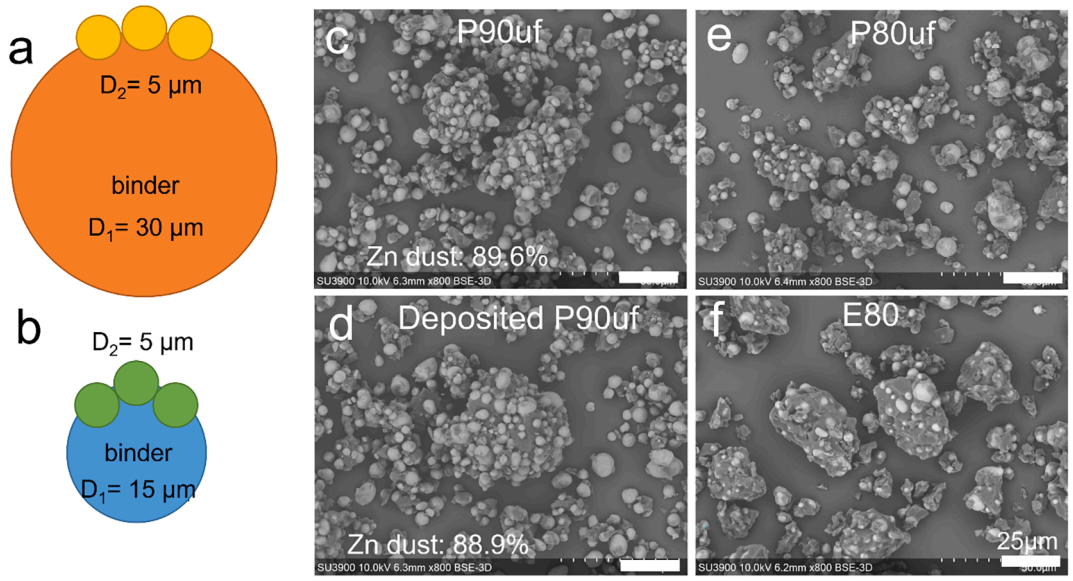

Fig. 2. Bonding pattern between zinc particles and (a) a coarse binder particle and (b) an ultrafine one. SEM images of (c) P90uf, (d) Deposited P90uf, (e) P80uf and (f) extruded E80 powder. (Scale bar is 25 μm).

$$N_{zinc} = \frac{\pi \times D_{binder}^2}{\frac{1}{4} \times \pi \times D_{zinc}^2} \quad (5)$$

Where D_{binder} is the D50 of the binder particles. D_{zinc} is the D50 of the zinc particles. The loading weight of zinc dust on binder particles (η) can be calculated with the equation:

$$\eta = \frac{\frac{\pi}{6} \times D_{zinc}^3 \times \rho_{zinc} \times N_{zinc}}{\frac{\pi}{6} \times D_{binder}^3 \times \rho_{binder}} \quad (6)$$

Where ρ_{zinc} is the density of zinc dust (7.1 g/cm^3) and ρ_{binder} is the density of polyester binder (1.0 g/ cm^3). The weight ratio of zinc in the bonded powder (τ) can be calculated with the equation:

$$\tau = \frac{\frac{\pi}{6} \times D_{zinc}^3 \times \rho_{zinc} \times N_{zinc}}{\frac{\pi}{6} \times D_{binder}^3 \times \rho_{binder} + \frac{\pi}{6} \times D_{zinc}^3 \times \rho_{zinc} \times N_{zinc}} \times 100\% \quad (7)$$

The loading capacity of zinc particles on binder for different zinc-rich coatings is listed in Table 2. When binder particles have an average size of 13.0 μm, the theoretical limit of zinc content is 91.6 wt%. For fine and coarse binder with average particle size of 28.6 μm and 48.9 μm, the limits are 83.2 wt% and 74.4 wt%, respectively.

Fig. 2c shows the morphology of the press-bonded P90uf powders. Most of the bonded particles are in a raspberry-like zinc-on-binder structure. Very few unbonded zinc particles were found (Fig. S3). In addition, the deposited powder showed a bonding pattern similar to that of the original P90uf powder (Fig. 2d), which indicates that the zinc particles were generally well bonded with the binder. There were also a few unbonded zinc particles in the deposited powders, which means that a small amount of unbonded zinc particles showed no apparent influence on the bonding performance. Zinc dust particles, due to electrostatic forces, can also deposit on a grounded panel. (Fig. S4).

While the powder morphology offered qualitative evaluation of the bonding performance between zinc and binder particles, chemical composition analysis could provide quantitative analysis on the zinc content. For the P90uf powder, the incorporated zinc dust was 90 wt%. The zinc content in the prepared powder is expected to be the same. As measured with the excessive acid, the zinc dust content in the obtained powder after press bonding was 89.6%. Once the powder was sprayed and deposited on the targeted substrate, the zinc dust content slightly decreased to 88.9%, although the difference could be ignored. This finding indicates that zinc content can be maintained with press bonding.

Table 2
The loading capacity of zinc on binder in an ideal bonding pattern.

Coating	Zinc/μm	Binder/μm	N_{zinc}	η	τ
Ultrafine	5	13.0	27	10.92	91.6%
Fine	5	28.6	131	4.97	83.2%
Coarse	5	48.9	383	2.90	74.4%

Zinc-rich coating films with different zinc contents were fabricated to evaluate the tunability of zinc content in zinc-rich powder coatings with press bonding. As shown in Fig. 2e and Fig. S3, the powder morphology of P80uf was similar to, but had fewer zinc particles on the binder particles than, that of P90uf. In P80C, the zinc particles were densely packed and embedded into the surface with a few unbonded zinc particles (Fig. S5), indicating that the particles were generally well bonded like P80uf and P90uf. Fig. 2f presents the extruded zinc-rich powder particles. Most zinc particles were wrapped inside the binder while some were half exposed. It is noticeable that there were also some poorly bonded zinc particles (the bright particles as shown in Fig. 2f and Fig. S3d).

3.2. Surface morphology

Light mirror reflection is an effective method to evaluate the surface qualities. Stronger mirror reflection translates to a smoother surface. The inset in Fig. 3a shows the gloss of the fabricated coating panels under light. The E80 had the highest gloss, with a 60° gloss of about 23, higher than the press-bonded coating films. All the zinc-rich coating films showed lower gloss than the extruded coating film with the P90uf having very rough surface and almost no gloss.

CLSM is efficient to characterize surface morphology and provide quantitative analysis [34,35]. In this study, CLSM was employed to characterize the surface roughness. As shown in Fig. 3c and 3d, both coating films included considerable hills and valleys of tens of micrometers in a relatively large scanning area (0.96 mm × 0.96 mm). The press-bonded coating films displayed more and higher hills than the extruded one. In addition, E80 had lower surface roughness than P80uf. The arithmetic average surface roughness (Sa) of E80 was lower (1.7 μm) than that for P80uf (2.2 μm). The maximum height (the sum of the largest peak height value and the largest valley depth value) for E80 was also lower (18.0 μm) than that for P80uf (21.0 μm) (Fig. 3b), which

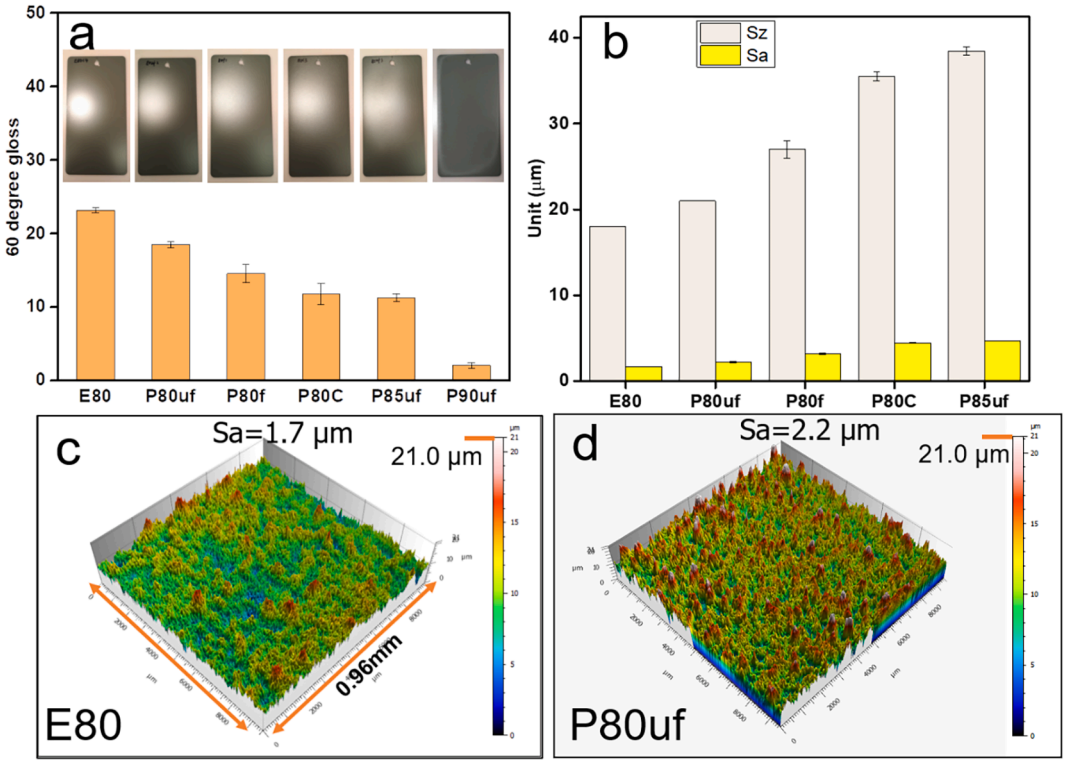

Fig. 3. (a) 60-degree gloss of the different coatings. Insets are the pictures of the coated panels (8 cm × 15 cm) under visible light. (b) Surface roughness of the extruded and press-bonded coating films. 3D CLSM images of the (c) E80 and (d) P80uf coating films.

indicates that the press-bonded coating film had higher surface roughness than the extruded one. Furthermore, the surface roughness of the obtained coating films increased with the size of binder particle. As shown in Fig. S6, the hills on the surface became higher and broader for P80f (D50 of binder was 30 μm) and P80C (D50 of binder was 46 μm). The Sa increased to 2.2 μm (P80f) and 4.5 μm (P80C), respectively. In addition, P85uf showed higher surface roughness (Sa = 4.7 μm and Sz = 38.0 μm) than the coating films with 80 wt% zinc.

3.3. Cross-sectional morphology and zinc dispersion

In a zinc-rich coating film, the percolation, i.e., a good electrical contact between the zinc particles and the steel, allows the substrate to benefit from the cathodic protection from the zinc [15,36-38]. Higher zinc content results in better connection. On the other hand, the coating structures are also a critical aspect. For example, coating films with a lower barrier effect permit rapid penetration of electrolyte and early and quick dissolution of zinc particles [11].

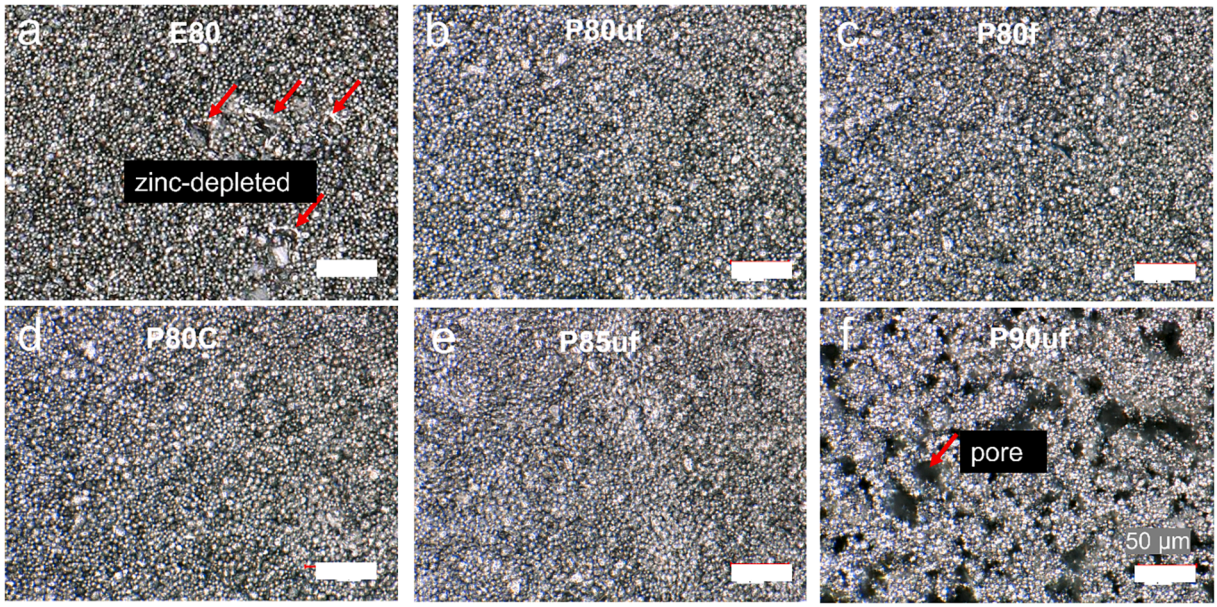

Fig. 4. OM images of the surface of the zinc-rich powder coatings. (a) E80, red arrows indicate zinc depleted areas. (b) P80uf, (c) P80f, (d) P80C, (e)P85uf and (f) P90uf. Red arrow indicates pore in the film. (Scale bar is 50 μm).

OM, SEM and Micro-CT were employed to characterize the dispersion of zinc particles and voids inside a coating film. OM was used to view the dispersion of shiny zinc particles because the binder is transparent. The top views (OM), side views (SEM) and 3D global views (micro-CT) of the different ZRPCs are shown in Figs. 4, 5 and 6, respectively. For E80, the zinc particles were generally uniformly packed inside the coating film (Fig. 5a), but there were also some zinc-depleted areas as found from the top view (Fig. 4a and Fig. 6a). Some zinc-depleted areas were as large as 80 μm wide (Video S1). This finding corresponds to the problem of powder homogeneity in industry when the zinc content is higher than 70 wt%. Indeed, it is difficult to fabricate consistent zinc-rich particles with equivalent amount of binder, additives and zinc dust [10].

P80uf showed a more uniform dispersion of zinc particles than E80 from the top views (Fig. 4b, Fig. 6b and 6c, Video S2), although there were more voids inside (red arrows in Fig. 5f and 5 g). P80f and P80C displayed apparent zinc-depleted areas (Fig. 5c and 5d). P85uf demonstrated denser packing of zinc particles (Fig. 4e and 5e) than the coating films with 80 wt% zinc, but its surface had apparent fluctuations. P90uf had a porous surface (Fig. 4f), although almost all the zinc particles joined together with a point-to-point connection (Fig. S7). This porous zinc-rich coating film is of no practical use, but it at least formed a plain film. Further studies to improve the surface qualities are undergoing.

In general, the differences in gloss, surface and cross-sectional morphologies can be attributed to three reasons. The first one is the zinc content. The large amount of zinc particles in the coating powders can dramatically increase the melt viscosity during extrusion and curing and deteriorate the leveling of the coating films during curing. As a result, the extrusion cannot normally operate and uniformly disperse the zinc particles for E80, which is a common problem for zinc-rich powder coatings with zinc content over 70 wt% [10]. When we were processing the E80 powder sample, the lab-scale powder coating extruder was often stuck, even if the extruder was working at its full power and at a relatively high extrusion temperature (120 °C). The high zinc contents induced poor leveling leaving voids and pores inside the obtained coating films, and hills and valleys on the film surfaces (Figs. 3, 4 and 5) for all the zinc-rich coating films. Such effects were more apparent for P85uf and P90uf where binders only account for 10–15 wt% in the coating powders.

The second one is the unique press bonding process and the raspberry-like zinc-on-binder bonding structure (Fig. 2). In press bonding, zinc particles were free from extrusion. They were firmly embedded into the binder particle surface and reached a zinc content of about 90 wt% with ultrafine binder particles. During curing, zinc particles needed to migrate to the zinc depleted areas in the melted binder to form a uniform dispersion inside the coating film. But the total migration distance is limited due to the gradually increased viscosity caused by crosslinking reactions between resin and curing agent. As a result, the insufficient leveling caused more voids inside the coating films (Figs. 5 and 6), higher surface roughness (Fig. 4) and lower gloss (Fig. 3) for the press-bonded coating films than for extruded ones.

The third one is the binder particle size. As there was only one layer of embedded zinc particles on each binder particle, smaller binder particles resulted in more uniform mixing of zinc with binder and led to smaller bonded particles. The smaller coating particles, due to higher charge to mass ratio, usually deposited more uniformly during spraying [9,39-41]. In addition, the smaller particles can quickly melt and coalesce with each other, fill the voids inside the coating film during curing, and form coating films with smoother surfaces and fewer inner voids. As a result, in P80C, where the largest particle can reach 2 times its median particle size (46 μm), large zinc depleted areas of about 30–40 μm wide formed (Fig. 5d). P80uf, benefited from the small particle size (D50 was 13 μm), had uniform zinc dispersion (Figs. 4, 5 and 6), more uniform than E80.

3.4. Anti-corrosive performances

Open circuit potential (OCP) measurement is a common method to evaluate the electrochemical properties of a zinc-rich coating film [22,42,43]. It is well accepted that the steel substrate is cathodically protected by a zinc-rich coating film when the OCP is more negative than − 0.780 V/SCE [44]. The cathodic protection period (CPP) can be estimated as the period at which the OCP of the coated steel remains lower than − 0.780 V/SCE (the red dish line in Fig. 7). The OCP demonstrated a major fluctuation at the beginning of immersion (1–20 days), then remained stable at around −0.950 V before slowly rising

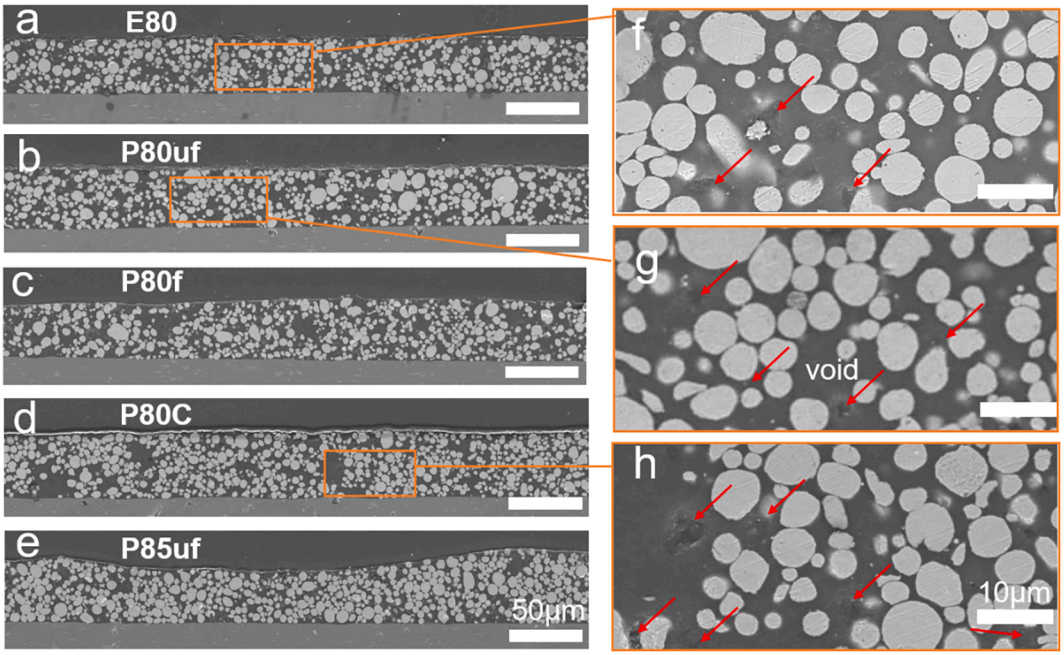

Fig. 5. SEM images of (a) extruded and press-bonded (b-e) coating films. (f-h) Magnified images of (a) (b) and (d). Red arrows indicate voids inside the coating film. (Scale bar is 50 μm in a, b, c, d, e and 10 μm in f, g and h).

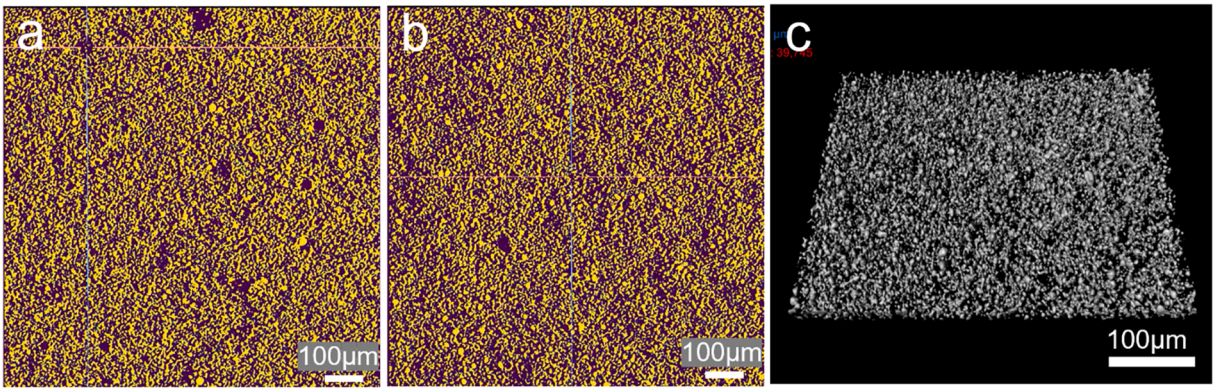

Fig. 6. One projection of the inner structure of the (a) E80 and (b) P80uf coating films. (c) 3D micro-CT image of P80uf.

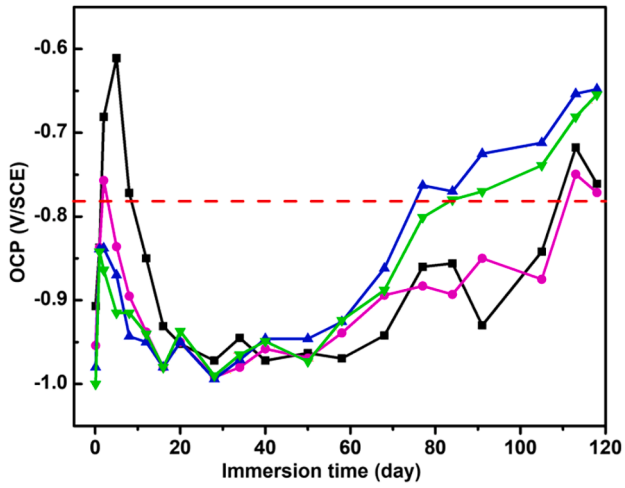

Fig. 7. OCP of the coatings at different time of immersion.

again. This fluctuation is mainly attributed to the formation of corrosion products on the coating surface which blocked the electrical connection paths, as a thin layer of white corrosion products was noticeable after 5 days of immersion.

E80 had a major fluctuation of about 8 days above −0.780 V/SCE and a total CPP of 101 days, while P80uf demonstrated a minor fluctuation of only 1 day and therefore a total CPP of 110 days. The longer CPP of P80uf indicates that P80uf had better active protection than E80. All the coating panels presented a CPP longer than 70 days, much longer than the 40 days reported for a 97 wt% zinc-rich epoxy-polyamide coating [8] and behaved more like the inorganic zinc-rich ethyl silicate coatings with 84 wt% zinc [8], indicating the great potential of zinc-rich powder coatings for long corrosion protection.

To analyze zinc activities during cathodic protection, potentiodynamic polarization tests were conducted. Corrosion voltage (E_{corr}) and corrosion current density (i_{corr}) were fitted by the electrochemical software Cview. i_{corr} represents the zinc corrosion activities in the coatings during cathodic protection. R_p represents the polarization resistance of coatings obtained from the slope of the potentiodynamic polarization curves over the narrow potential range of ± 20 mV relative to E_{corr}. R_p is inverse to i_{corr}. The results from polarization tests (Fig. 8) show that the press-bonded coating films demonstrated about half to one order of higher i_{corr} and lower R_p than E80, implying faster zinc corrosion in the press-bonded coating films. However, there was no visible iron corrosion spots until cathodic protection failed (after 110 days), when minor brown corrosion products were observed under OM and iron element was detected under SEM/EDS (Fig. S8). This finding indicates that zinc provided sufficient protection for steel during cathodic protection. After immersion tests, the press-bonded samples showed more white corrosion products accumulated on the coating film surfaces than E80 (Fig. S9). P80uf presented a thicker layer of zinc corrosion products (about 6.0 μm) than did E80 (about 4.4 μm) and had Cl^- prevailed into deeper areas of the coating film (Fig. 9). As E80 (zinc: 79.3 wt %) had similar zinc dust content with P80uf (79.8 wt%), P80uf demonstrated higher zinc utilization.

In Fig. 8f, R_p of the zinc-rich samples showed a downward trend at the beginning and an upward trend at the later time of immersion. To evaluate the electrochemical behavior of the zinc-rich coatings during immersion, EIS measurements were conducted.

In EIS spectrum, a phase angle closer to −90° in the high frequency region (10^3 – 10^5 Hz) indicates better capacitive property of the coating, and a higher impedance at the low frequency (10^0 – 10^{-2} Hz) suggests better barrier properties and therefore slower electrolyte ingress [29,45,46]. Usually, the impedance at 0.01 Hz is a semiquantitative indicator for the barrier properties of organic coating films [29,47,48]. Fig. 10a-d show the impedance module and phase angle of the E80 and P80uf as a function of frequency during immersion. For both E80 and P80uf, the impedance at low frequency gradually decreased with immersion time due to the rapid ingress of electrolyte through the voids and defects of the coating films (Fig. 5). Zinc started corrosion and protected the steel substrate. P80uf demonstrated lower impedance (2.08×10^6 Ω•cm^2) at 0.01 Hz and therefore faster electrolyte ingress than E80 (1.12×10^7 Ω•cm^2), corresponding to the relatively high i_{corr} and low R_p of P80uf coatings (Fig. 8e-f).

After about 30–40 days of immersion, the impedance started to increase. This was attributed to the accumulation of zinc corrosion products, which sealed the pores inside the coating films [2,49]. The impedance of P80uf finally exceeded that of E80 after about 65 days and almost reached its original values by the end of immersion as shown in Fig. 10e. This finding indicates that P80uf coating film with lower barrier effects had higher sealing effects than E80.

EIS data was further fitted using Zview software with equivalent electrical circuits (EEC) to quantitatively evaluate the time-dependent performances of the coatings. In the EEC, R_s relates to the solution resistance. R_{pore} and R_{ct} represent the pore resistance and the charge transfer resistance. The constant phase element (CPE) stands for the difference from pure capacitance, referring to as the dispersion effect. The difference degree from an ideal capacitive behavior can be expressed by an exponent (α). CPE_{coat} and CPE_{dl} denote the coating capacitance and double-layer capacitance, respectively. For an ideal resistor, α = 0; and for an ideal capacitance (CPE = C), α = 1 [50,51]. The warburg element (W_s) represents diffusion process in the coating film [52]. In the beginning 30–40 days, both ingress of electrolyte and diffusion of zinc corrosion products prevailed in the coating films. Then the mass transfer process could be expressed with the EEC in the inset of Fig. 10f. After about 40 days when accumulation of corrosion products (increase of impedance at 0.01 Hz) prevailed the corrosion process, the

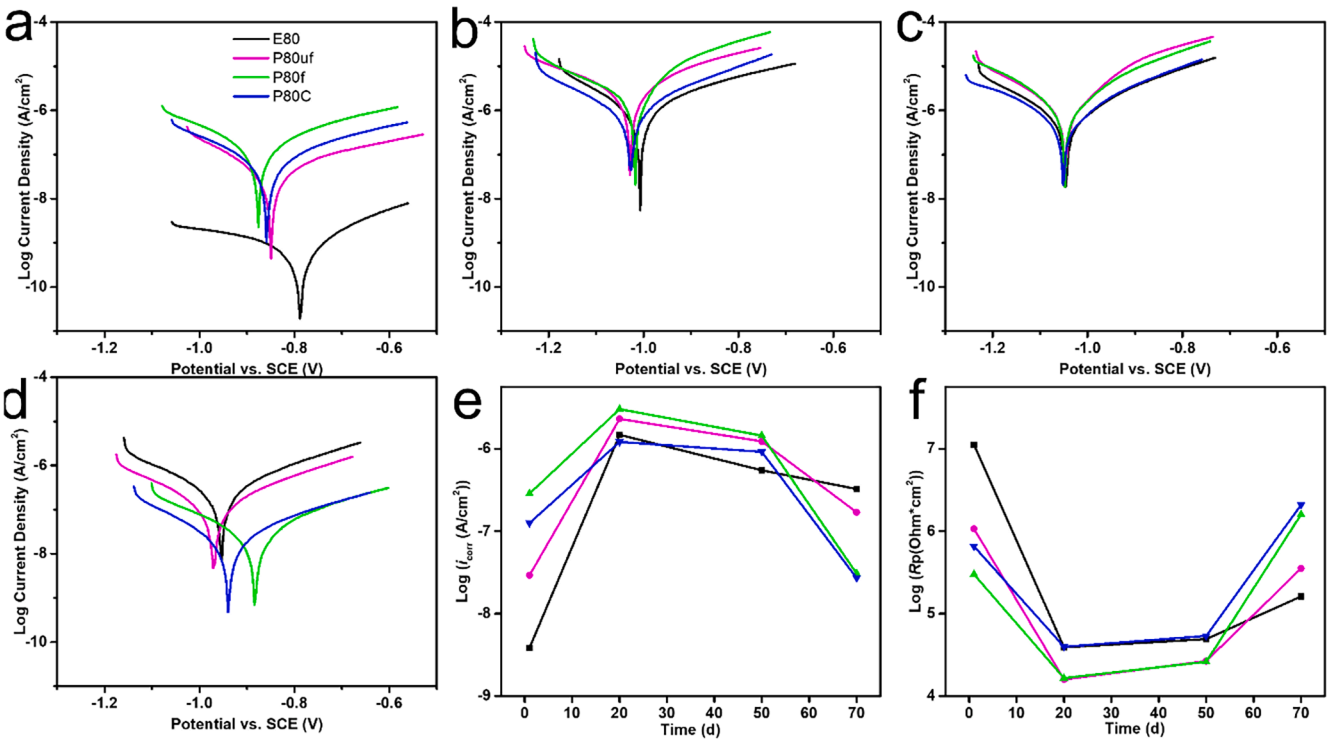

Fig. 8. Polarization curves of the coatings after different time of immersion. (a) 1 day, (b) 20 days, (c) 50 days, (d) 70 days. (e) The change of corrosion current density and (f) polarization resistance with time.

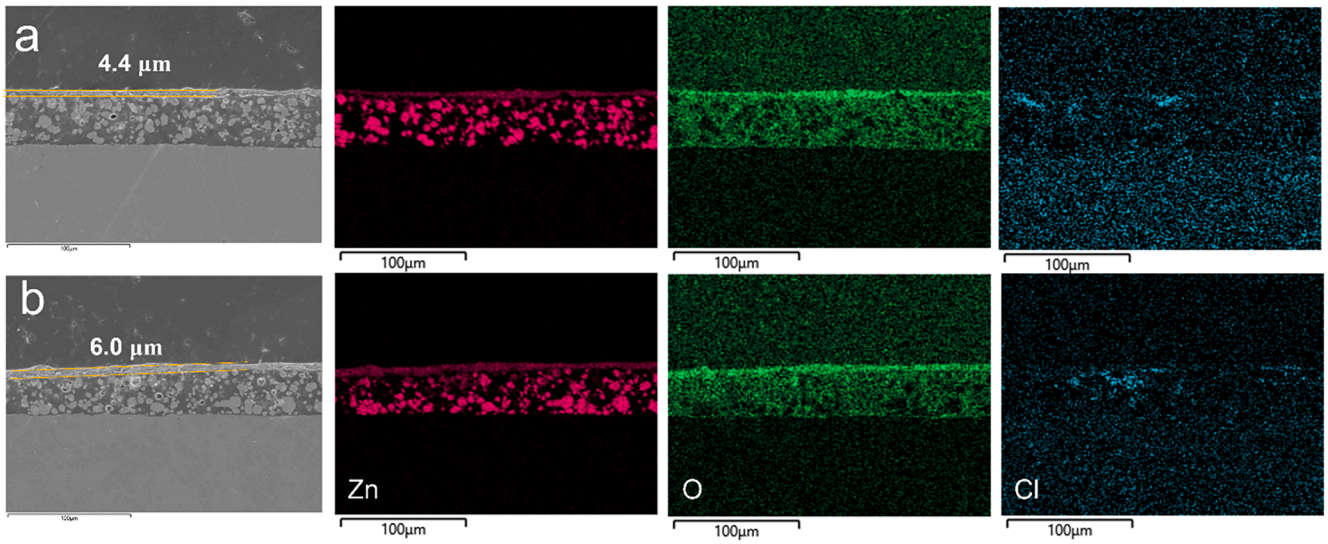

Fig. 9. SEM images of (a) E80 and (b) P80uf after 110 days of immersion in 3.5 % NaCl and their corresponding EDS maps. The numbers on panels a and b refer to the corrosion product layer thickness in each case. (Scale bar is 100 μm).

EEC in Fig. 10f cannot provide good fitting. Then a Randles-like EEC [10,53] as shown in the inset of Fig. 10*h* was used. The fitted results for each element over immersion time were shown in Table S1 and S2 and Fig. 10f-h.

The evolution of R_{pore}, R_{ct} and the resistive component in W_s were used to assess the barrier properties of the coating films. It is obvious that all these parameters dropped to their lowest after about 30–40 days of immersion and then increased gradually, except for R_{ct}. This trend is the same for the impedance at 0.01 Hz (Fig. 10e) and R_p (Fig. 8f), although R_{pore} was usually one order of magnitude lower than the impedance at 0.01 Hz and the resistive component in W_s. In addition, it should be noted that P80uf with one order of magnitude lower R_{pore} than E80 at the beginning, reached a value of 7.70×10^4 Ω•cm^2, higher than that for E80 (4.87×10^4 Ω•cm^2) after immersion, demonstrating the strong pore-sealing effect of P80uf.

Salt spray tests were conducted to analyze the overall corrosion resistance of the coating panels. The zinc-rich powder coating panels presented few brown rust sites after 500 h of exposure, and they had apparent rust sites after 1000 h (Fig. S10). After 2500 h, P80uf demonstrated the narrowest creepage (about 1.3 mm) and the fewest localized corrosion sites (red arrows in Fig. 11), indicating that P80uf offered the best corrosion protection among all the prepared coating films. Localized corrosion sites on E80 were analyzed with OM and SEM. Fig. S11 shows that a minor localized corrosion site was observed in a

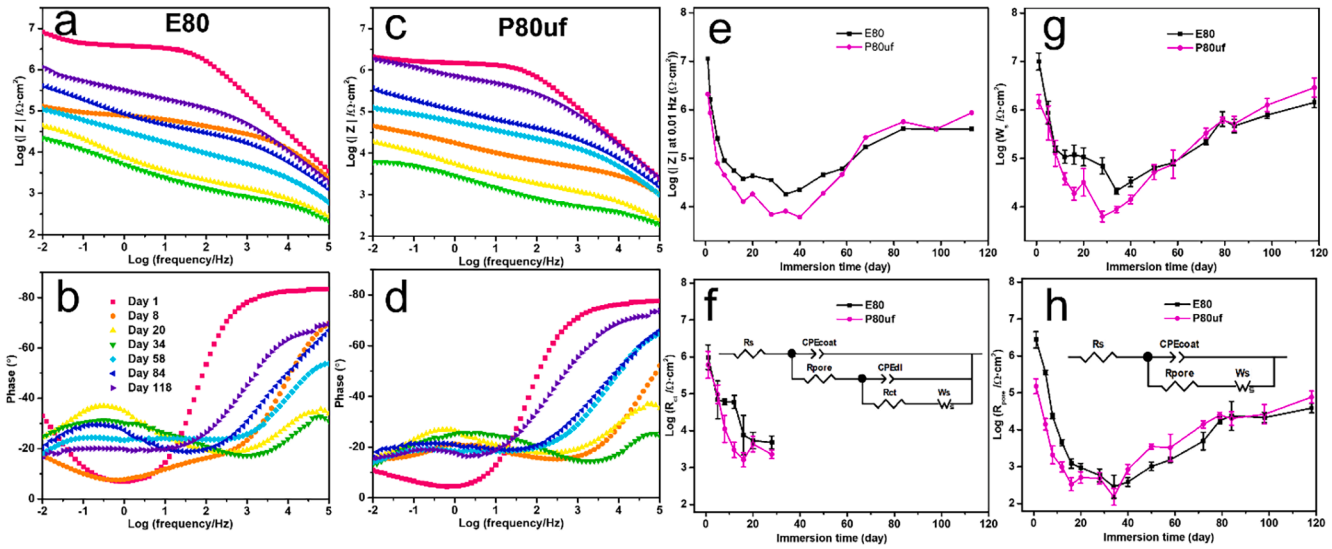

Fig. 10. (a) Bode-modulus plots and (b) Bode-phase plots of E80. (c) Bode-modulus plots and (d) Bode-phase plots of P80uf. (e) Impedance at 0.01 Hz, (f) R_{ct}, (g) resistive component in W_s (h) R_{pore} of P80uf and E80 versus immersion time in 3.5% NaCl solution. Insets in (f) and (h) are electrical equivalent circuits for fitting.

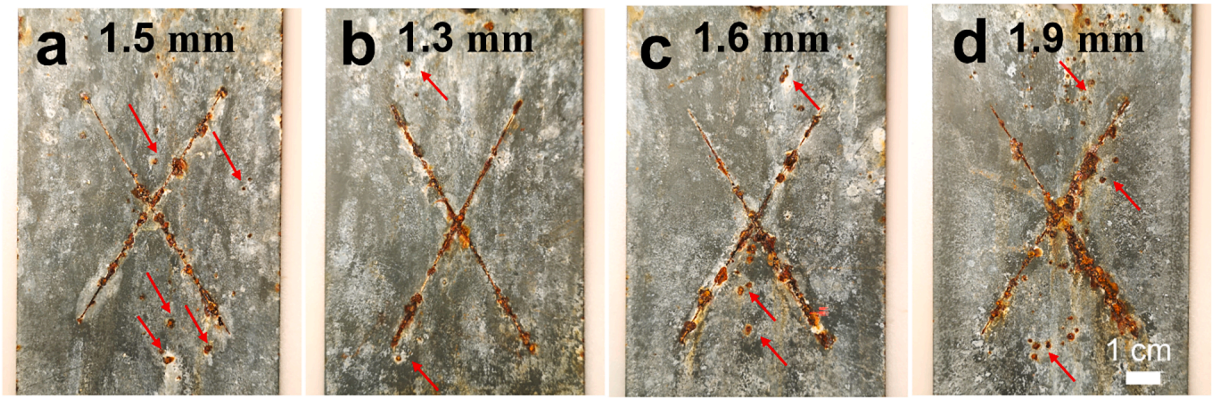

Fig. 11. Optical images of coating panels after 2500 h of salt spray tests. (a) E80, (b) P80uf, (c) P80f, (d) P80C. Red arrows indicate sites of localized corrosion away from the scribe marks. Numbers on each panel indicate the average corrosion creepage.

zinc-depleted area, while for a well-developed localized corrosion site (Fig. S12), the central part was more zinc-depleted than its surrounding areas. These findings indicate that localized corrosion was closely related to the non-uniform dispersion of zinc particles. P80uf demonstrated uniform zinc distribution therefore few localized corrosion spots.

The superior corrosion resistance of P80uf over E80 was attributed to three synergistic reasons. The first was the well bonding between zinc dusts and binder particles, which maintained the zinc concentration inside the fabricated coating films (Fig. 2). The second was the slightly higher surface roughness and lower barrier properties. These properties enabled easier electrolyte ingress, higher zinc corrosion rate, and higher zinc utilization (Figs. 2, 7 and 8) [10] (Fig. 8). The high zinc utilization not only maintained sufficient cathodic protection against corrosion (Fig. 7), but also produced more zinc corrosion products (Fig. 9), resulting in a better sealing of pores than in E80. The third was the uniform dispersion of zinc particles (Figs. 4, 5 and 6), which inhibited localized corrosion and realized an even corrosion progression (Fig. S10 and Fig. 11).

4. Conclusions

In summary, extrusion-free zinc-rich powder coatings were successfully fabricated for the first time by press bonding. The polyester clearcoat was first ground into ultrafine particles, mixed and press-bonded with zinc dust, ground and sieved to obtain coating powders. The zinc and binder particles formed a raspberry-like zinc-on-binder structure. The press bonding can maintain the zinc concentration in the fabricated coating films and the zinc dust content can reach about 90 wt % in the coating powders. The press-bonded ZRPC with 80 wt% zinc demonstrated slightly higher surface roughness, but more uniform dispersion of zinc particles and higher zinc utilization than the extruded one with the same zinc content. As a result, the press-bonded coating films demonstrated a longer cathodic protection period (110 days), higher sealing effect, narrower corrosion creepage, and fewer localized corrosion sites. This study contributes to the fabrication of extrusion-free zinc-rich powder coatings with zinc content higher than 70 wt% and extends the applications of powder coatings in heavy-duty anticorrosive coating industries.

Declaration of Competing Interest

The authors declare that they have no known competing financial interests or personal relationships that could have appeared to influence the work reported in this paper.

Acknowledgement

Thanks for the fundings from China Scholarship Council (CSC) (No.

201707040063), Natural Sciences and Engineering Research Council of Canada (Grant RGPIN-2018-06256 and RGPIN-2018-06672), Hundred Talent Project (E155F207) and Zhengzhou University as well as the technical supports from the Department of Chemistry and Surface Science Western at Western University.

Appendix A. Supplementary data

Supplementary data to this article can be found online at https://doi.org/10.1016/j.cej.2022.135925.

References

[1] J.R. Vilche, E.C. Bucharsky, C.A. Giúdice, Application of EIS and SEM to evaluate the influence of pigment shape and content in ZRP formulations on the corrosion prevention of naval steel, Corros. Sci. 44 (2002) 1287–1309, https://doi.org/10.1016/S0010-938X(01)00144-5.
[2] P.A. Sørensen, S. Kiil, K. Dam-Johansen, C.E. Weinell, Anticorrosive coatings: A review, J. Coat. Technol. Res. 6 (2009) 135–176, https://doi.org/10.1007/s11998-008-9144-2.
[3] V.-D. Vuong, A. Quang Vu, H.-N. Nguyen, T. Van Le, DIFFERENT BEHAVIORS OF ZINC RICH PAINT AGAINST CORROSION IN ATMOSPHERIC ZONE AND TIDAL ZONE OF INDUSTRIAL PORT ENVIRONMENT, Vietnam Journal of Science and Technology. 55 (2017) 194–194. 10.15625/2525-2518/55/5B/12226.
[4] D. Wang, I. Dizvay, E. Sikora, B.A. Shaw, N. Al-Jassem, Development of New Multifunctional Coatings for Protection Against Erosion and Corrosion in Qatar Oil and Gas Production, ECS, Meeting Abstracts. MA2014-02 (2014) 778, https://doi.org/10.1149/MA2014-02/13/778.
[5] C.E. Weinell, A.R. Black, P.K. Nielsen, New developments in coatings for extended lifetime for offshore wind structures, in, NACE - International Corrosion Conference Series (2017).
[6] C.M. Abreu, M. Izquierdo, M. Keddam, X.R. Nóvoa, H. Takenouti, Electrochemical behaviour of zinc-rich epoxy paints in 3% NaCl solution, Electrochim. Acta 41 (1996) 2405–2415, https://doi.org/10.1016/0013-4686(96)00021-7.
[7] J. Ruf, KORROSION-SCHUTZ DURCH LACKE UND PIGMENTE., Colomb, 1972.
[8] S. Feliu, R. Barajas, J.D. Bastidas, M. Morcillo, Mechanism of cathodic protection of zinc-rich points by electrochemical impedance spectroscopy. I: Galvanic stage, JCT, J. Coat. Technol. 61 (1989).
[9] A.G. Bailey, The science and technology of electrostatic powder spraying, transport and coating, J. Electrostat. 45 (1998) 85–120, https://doi.org/10.1016/S0304-3886(98)00049-7.
[10] H. Marchebois, S. Joiret, C. Savall, J. Bernard, S. Touzain, Characterization of zinc-rich powder coatings by EIS and Raman spectroscopy, Surf. Coat. Technol. 157 (2002) 151–161, https://doi.org/10.1016/S0257-8972(02)00147-0.
[11] H. Marchebois, S. Touzain, S. Joiret, J. Bernard, C. Savall, Zinc-rich powder coatings corrosion in sea water: Influence of conductive pigments, Prog. Org. Coat. 45 (2002) 415–421, https://doi.org/10.1016/S0300-9440(02)00145-5.
[12] C.H. Hare, S.J. WRIGHT, ANTI-CORROSIVE PRIMERS BASED ON ZINC FLAKE, (1982).
[13] A. Meroufel, S. Touzain, EIS characterisation of new zinc-rich powder coatings, Prog. Org. Coat. 59 (2007) 197–205, https://doi.org/10.1016/j.porgcoat.2006.09.005.
[14] S. Touzain, Accelerated aging of zinc-rich powder coatings containing different conductive pigments, Powder Coating Pigments. (2009) 1–6.
[15] A. Meroufel, C. Deslouis, S. Touzain, Electrochemical and anticorrosion performances of zinc-rich and polyaniline powder coatings, Electrochim. Acta 53 (2008) 2331–2338, https://doi.org/10.1016/j.electacta.2007.09.056.
[16] F.T. Shirehjini, I. Danaee, H. Eskandari, S. Nikmanesh, D. Zarei, Improvement of the sacrificial behavior of zinc in scratches of zinc-rich polymer coatings by incorporating clay nanosheets, Materialpruefung/Materials Testing. 59 (2017) 682–688, https://doi.org/10.3139/120.111057.
[17] F.T. Shirehjini, I. Danaee, H. Eskandari, D. Zarei, Effect of Nano Clay on Corrosion Protection of Zinc-rich Epoxy Coatings on Steel 37, J. Mater. Sci. Technol. 32 (2016) 1152–1160, https://doi.org/10.1016/j.jmst.2016.08.017.
[18] K. Schaefer, A. Miszczyk, Improvement of electrochemical action of zinc-rich paints by addition of nanoparticulate zinc, Corros. Sci. 66 (2013) 380–391, https://doi.org/10.1016/j.corsci.2012.10.004.
[19] N. Arianpouya, M. Shishesaz, M. Arianpouya, M. Nematollahi, Evaluation of synergistic effect of nanozinc/nanoclay additives on the corrosion performance of zinc-rich polyurethane nanocomposite coatings using electrochemical properties and salt spray testing, Surf. Coat. Technol. 216 (2013) 199–206, https://doi.org/10.1016/j.surfcoat.2012.11.036.
[20] S. Teng, Y. Gao, F. Cao, D. Kong, X. Zheng, X. Ma, L. Zhi, Zinc-reduced graphene oxide for enhanced corrosion protection of zinc-rich epoxy coatings, Prog. Org. Coat. 123 (2018) 185–189, https://doi.org/10.1016/j.porgcoat.2018.07.012.
[21] Z. Song, B. Qian, Effect of graphene on the electrochemical protection of zinc-rich coatings, Mater. Corros. 69 (2018) 1854–1860, https://doi.org/10.1002/maco.201810312.
[22] H. Hayatdavoudi, M. Rahsepar, A mechanistic study of the enhanced cathodic protection performance of graphene-reinforced zinc rich nanocomposite coating for corrosion protection of carbon steel substrate, J. Alloy. Compd. 727 (2017) 1148–1156, https://doi.org/10.1016/j.jallcom.2017.08.250.
[23] S.M. Park, M.Y. Shon, Effects of multi-walled carbon nano tubes on corrosion protection of zinc rich epoxy resin coating, J. Ind. Eng. Chem. 21 (2015) 1258–1264, https://doi.org/10.1016/j.jiec.2014.05.042.
[24] H.Y. Wu, S. Lee, J.Y. Wang, Solid-state bonding of iron-based alloys, steel-brass, and aluminum alloys, J. Mater. Process. Technol. 75 (1998) 173–179, https://doi.org/10.1016/S0924-0136(97)00323-3.
[25] G. Min, J.M. Lee, S.B. Kang, H.W. Kim, Evolution of microstructure for multilayered Al/Ni composites by accumulative roll bonding process, Mater. Lett. 60 (2006) 3255–3259, https://doi.org/10.1016/j.matlet.2006.03.001.
[26] C. Hildebrandt, S.R. Gopireddy, R. Scherließ, N.A. Urbanetz, Investigation of powder flow within a pharmaceutical tablet press force feeder – A DEM approach, Powder Technol. 345 (2019) 616–632, https://doi.org/10.1016/j.powtec.2019.01.040.
[27] S. Amirkhanlou, M. Ketabchi, N. Parvin, S. Khorsand, R. Bahrami, Accumulative press bonding; a novel manufacturing process of nanostructured metal matrix composites, Mater. Des. 51 (2013) 367–374, https://doi.org/10.1016/j.matdes.2013.04.032.
[28] W. Liu, H. Zhang, Y. Shao, H. Zhang, J. Zhu, Produce various powder coated surfaces with stable metal shine via microwave energy, Prog. Org. Coat. 154 (2021), 106199, https://doi.org/10.1016/J.PORGCOAT.2021.106199.
[29] J.R. Scully, Electrochemical Impedance of Organic-Coated Steel: Correlation of Impedance Parameters with Long-Term Coating Deterioration, J. Electrochem. Soc. 136 (1989) 979–990, https://doi.org/10.1149/1.2096897.
[30] E. Spyrou, Powder Coatings Chemistry and Technology, 3rd ed., Vincentz Network, 2012. 10.1515/9783748602361.
[31] W. Liu, J. Fu, H. Zhang, Y. Shao, H. Zhang, J. Zhu, Cold bonding method for metallic powder coatings, Materials. 11 (2018) 2086, https://doi.org/10.3390/ma11112086.
[32] W. Liu, H. Zhang, Y. Shao, H. Zhang, J. Zhu, Preparation of aluminium metallic pigmented powder coatings with high color stability using a novel method: Microwave bonding, Prog. Org. Coat. 147 (2020), 105787, https://doi.org/10.1016/j.porgcoat.2020.105787.
[33] K.H. Kim, M. Watanabe, S. Kuroda, Bonding mechanisms of thermally softened metallic powder particles and substrates impacted at high velocity, Surf. Coat. Technol. 204 (2010) 2175–2180, https://doi.org/10.1016/j.surfcoat.2009.12.001.
[34] J. Huang, M. Yang, H. Zhang, J. Zhu, Solvent-Free Fabrication of Robust Superhydrophobic Powder Coatings, ACS Appl. Mater. Interfaces 13 (2021) 1323–1332, https://doi.org/10.1021/acsami.0c16582.
[35] O. Schneider, G.O. Ilevbare, J.R. Scully, R.G. Kelly, Confocal laser scanning microscopy as a tool for in situ monitoring of corrosion underneath organic coatings, Electrochem. Solid-State Lett. 4 (2001) 3–7, https://doi.org/10.1149/1.1413703.
[36] A. Gergely, Z. Pászti, J. Mihály, E. Drotár, T. Török, Galvanic function of zinc-rich coatings facilitated by percolating structure of the carbon nanotubes, Part II: Protection properties and mechanism of the hybrid coatings, Progress in Organic Coatings. 77 (2014) 412–424, https://doi.org/10.1016/j.porgcoat.2013.11.004.
[37] H. Marchebois, M. Keddam, C. Savall, J. Bernard, S. Touzain, Zinc-rich powder coatings characterisation in artificial sea water EIS analysis of the galvanic action, Electrochim. Acta 49 (2004) 1719–1729, https://doi.org/10.1016/j.electacta.2003.11.031.
[38] A. Gergely, I. Bertóti, T. Török, É. Pfeifer, E. Kálmán, Corrosion protection with zinc-rich epoxy paint coatings embedded with various amounts of highly dispersed polypyrrole-deposited alumina monohydrate particles, Prog. Org. Coat. 76 (2013) 17–32, https://doi.org/10.1016/j.porgcoat.2012.08.005.
[39] Z. Li, C. Zhang, J. Zhu, Numerical study of the effect of particle size on the coating efficiency and uniformity of an electrostatic powder coating process, Can. J. Chem. Eng. 83 (2005) 882–888, https://doi.org/10.1002/cjce.5450830510.
[40] E. Spyrou, Powder coatings – chemistry and technology, 3rd ed., Vincentz Network, 2012: pp. 248-249. 10.1016/s1364-5439(04)00135-2.
[41] X. Meng, J. Zhu, H. Zhang, The characteristics of particle charging and deposition during powder coating processes with ultrafine powder, J. Phys. D Appl. Phys. 42 (2009), https://doi.org/10.1088/0022-3727/42/6/065201.
[42] S. Shreepathi, P. Bajaj, B.P. Mallik, Electrochemical impedance spectroscopy investigations of epoxy zinc rich coatings: Role of Zn content on corrosion protection mechanism, Electrochim. Acta 55 (2010) 5129–5134, https://doi.org/10.1016/j.electacta.2010.04.018.
[43] A. Gergely, É. Pfeifer, I. Bertóti, T. Török, E. Kálmán, Corrosion protection of cold-rolled steel by zinc-rich epoxy paint coatings loaded with nano-size alumina supported polypyrrole, Corros. Sci. 53 (2011) 3486–3499, https://doi.org/10.1016/j.corsci.2011.06.014.
[44] J.F. Chmilar, Control of external corrosion on underground or submerged metallic piping systems, in: NACE International Standard Practice, 2010: pp. 1–12.
[45] J.R. Scully, S.T. Hensley, Lifetime prediction for organic coatings on steel and a magnesium alloy using electrochemical impedance methods, Corrosion. 50 (1994) 705–716, https://doi.org/10.5006/1.3293547.
[46] S. Touzain, Q. Le Thu, G. Bonnet, Evaluation of thick organic coatings degradation in seawater using cathodic protection and thermally accelerated tests, in, Progress in Organic Coatings, Elsevier (2005) 311–319, https://doi.org/10.1016/j.porgcoat.2004.09.007.
[47] H.P. Hack, Defect Area Determination of Organic Coated Steels in Seawater Using the Breakpoint Frequency Method, J. Electrochem. Soc. 138 (1991) 33, https://doi.org/10.1149/1.2085574.
[48] J.M. McIntyre, H.Q. Pham, Electrochemical impedance spectroscopy; a tool for organic coatings optimizations, Prog. Org. Coat. 27 (1996) 201–207, https://doi.org/10.1016/0300-9440(95)00532-3.

[49] R.N. Jagtap, P.P. Patil, S.Z. Hassan, Effect of zinc oxide in combating corrosion in zinc-rich primer, Prog. Org. Coat. 63 (2008) 389–394, https://doi.org/10.1016/j.porgcoat.2008.06.012.
[50] J. Zhong, G.-X. Zhou, P.-G. He, Z.-H. Yang, D.-C. Jia, 3D printing strong and conductive geo-polymer nanocomposite structures modified by graphene oxide, (2017). 10.1016/j.carbon.2017.02.102.
[51] E. Armelin, R. Whelan, Y.M. Martínez-Triana, C. Aleman, M.G. Finn, D.D. Díaz, Protective coatings for aluminum alloy based on hyperbranched 1,4-polytriazoles, ACS Appl. Mater. Interfaces 9 (2017) 4231–4243, https://doi.org/10.1021/ACSAMI.6B14174/SUPPL_FILE/AM6B14174_SI_003.AVI.
[52] J. Ding, H. Zhao, B. Xu, X. Zhao, S. Su, H. Yu, Superanticorrosive Graphene Nanosheets through π Deposition of Boron Nitride Nanodots, ACS Sustainable Chem. Eng. (2019), https://doi.org/10.1021/acssuschemeng.9b01796.
[53] S. Zhou, Y. Wu, W. Zhao, J. Yu, F. Jiang, Y. Wu, L. Ma, Designing reduced graphene oxide/zinc rich epoxy composite coatings for improving the anticorrosion performance of carbon steel substrate, Mater. Des. 169 (2019), 107694, https://doi.org/10.1016/J.MATDES.2019.107694.